PHYSICAL REVIEW B **84**, 035103 (2011)

Multicomponent magneto-optical conductivity of multilayer graphene on SiC

I. Crassee,[1] J. Levallois,[1] D. van der Marel,[1] A. L. Walter,[2,3] Th. Seyller,[4] and A. B. Kuzmenko[1]

[1]*Département de Physique de la Matière Condensée, Université de Genève, CH-1211 Genève 4, Switzerland*

[2]*Department of Molecular Physics, Fritz-Haber-Institut der Max-Planck-Gesellschaft, Faradayweg 4-6, D-14195 Berlin, Germany*

[3]*E. O. Lawrence Berkeley National Laboratory, Advanced Light Source, MS6-2100, Berkeley, California 94720, USA*

[4]*Lehrstuhl für Technische Physik, Universität Erlangen-Nürnberg, Erwin-Rommel-Strasse 1, D-91058 Erlangen, Germany*

(Received 18 April 2011; revised manuscript received 24 May 2011; published 15 July 2011)

Far-infrared diagonal and Hall conductivities of multilayer epitaxial graphene on the C face of SiC were measured using magneto-optical absorption and Faraday rotation in magnetic fields up to 7 T and temperatures between 5 and 300 K. Multiple components were identified in the spectra, including (i) a quasiclassical cyclotron resonance, originating from the highly doped graphene layer closest to SiC, (ii) transitions between low-index Landau levels (LLs), which stem from weakly doped layers, and (iii) a broad optical absorption background. Electron- and hole-type LL transitions are optically distinguished and shown to coexist. An electron-hole asymmetry of the Fermi velocity of about 2% was found within one graphene layer, while the Fermi velocity varies by about 10% across the layers. The optical intensity of the LL transitions is several times smaller than is theoretically expected for isolated graphene monolayers without electron-electron and electron-phonon interactions.

DOI: 10.1103/PhysRevB.84.035103 PACS number(s): 76.40.+b, 71.70.Di, 78.20.Ls, 68.65.Pq

I. INTRODUCTION

Graphene attracts much interest due to its intriguing physical properties and the potential for novel applications. Epitaxially grown graphene on SiC (Ref. 1) is particularly promising for large-scale production. The growth conditions of epitaxial graphene have been constantly improving in recent years, resulting in a macroscopic continuity of graphene layers and an enhanced mobility of charge carriers.[1–6] The electronic properties of epitaxial graphene grown on Si and C faces of SiC are markedly different.[7,8] Interestingly, multilayer epitaxial graphene produced on the carbon face shows a number of electronic features typical of isolated monolayer graphene, as revealed by infrared spectroscopy,[9] scanning tunneling microscopy (STM),[10,11] angle-resolved photoemission spectroscopy (ARPES),[12] and the quantum Hall effect.[13] In particular, the Landau levels in this material demonstrate a square-root dependence on the perpendicular magnetic field B and the level index n ($= 0, \pm 1, \ldots$):

$$E_n = E_D + \mathrm{sgn}(n)\sqrt{2e\hbar v_F^2 |nB|}, \qquad (1)$$

where v_F is the Fermi velocity and E_D is the Dirac-point energy. It is generally believed that this effective electronic interlayer decoupling is a result of twisted, non-Bernal stacking of the C-face-grown graphene layers. Significant progress in theoretical understanding of the influence of stacking on the electronic structure and Landau levels has been made.[14–22] However, no complete theory able to quantitatively predict the effect of twisting on the band structure at an arbitrary stacking angle exists at the moment even for bilayer graphene. In real samples, many layers are present with a random rotation between each pair of neighbors. Moreover, the substrate induces a strong variation of the Dirac-point energy E_D with respect to the chemical potential and therefore a very different density and mobility of carriers in different layers. More experiments are needed to understand the complex electronic structure of this system and establish favorable conditions for applications.

Infrared spectroscopy, which is a direct probe of charge dynamics, is well suited to studying carriers in graphene. Optical spectra contain contributions from all graphene layers, including those that are not seen by surface probes, such as ARPES and STM. In a recent work,[23] we measured the rotation of polarization of light passing through epitaxial graphene in a magnetic field, known as the Faraday effect. Being an optical analog of the dc Hall effect, the Faraday rotation reveals the sign of the charge carriers involved in various Landau-level (LL) transitions. Moreover, optical spectroscopy allows carriers to be distinguished on the base of their high-frequency dynamics, in contrast to the dc transport measurements. Here we present an extensive magneto-optical study of multilayer epitaxial graphene grown on the carbon side of SiC, by combining Faraday rotation measurements with transmission spectra and extracting both the diagonal and Hall optical conductivities. Different magneto-optical contributions are disentangled and studied quantitatively using a multicomponent cyclotron resonance (CR) model. This approach reveals a number of interesting properties of multiple charge carriers in multilayer graphene, for example, the simultaneous presence of both electron- and holelike components as well as the existence of carriers with different Fermi velocities. It also allows us to analyze the optical intensities of various transitions and make comparison to theoretical models. Finally, the dependence of optical spectra on temperature and environmental (surface) doping is studied.

II. TECHNIQUES

Rotationally stacked multilayer graphene on the carbon-terminated side of 6*H*-SiC was produced by hydrogen etching at 1450 °C and subsequent graphitization in an argon atmosphere at 1650 °C. The substrate has a thickness of 370 μm and a surface area of 10 × 10 mm^2. Undesirably

grown graphene was cleaned from the back side of the substrate using scotch tape. Using x-ray photoemission spectroscopy we estimated the number of graphene layers to be 5 ± 1 and checked that the back side was graphene-free. Additionally, we performed mid-infrared transmission microscopy over an area comparable to the total area used for the magneto-optical experiment using a spot size of 10×10 μm^2. We assume that each graphene layer absorbs 1.5% of the light at 1 eV, which is the value expected for monolayer graphene on SiC, provided that the chemical potential does not exceed 0.5 eV. This absorption value is lower than the absorption of 2.3% of free-standing graphene, because the refractive index of SiC is larger than 1. The infrared absorption shows a distribution peaked at seven layers with a full width at half maximum of 2.7 layers. The slightly larger number of layers revealed by infrared microscopy can be related to an underestimation of the absorption of one layer. Notably, both measurements show that at least four layers are present at any point of the sample.

We measured the Faraday rotation $\theta(\omega)$ and magneto-optical transmission $T(\omega)$ in the range of photon energies $\hbar\omega$ between 8 and 80 meV as described in Ref. 23. The optical transmission was measured with respect to a bare SiC substrate without graphene, which underwent similar hydrogen etching at 1450 °C as the graphitized sample. The optical spot had a diameter of 5 mm. Two series of measurements were performed: first by varying the temperature between 5 and 300 K at a fixed magnetic field of 3 T and then by varying the magnetic field from 0 to 7 T at a constant temperature of 5 K. Within each series, the optical absorption and the Faraday rotation were measured one after another with the shortest possible delay. During the experiments the sample was in a He gas flow; between the production and the experiments, as well as between the first and second series, it was stored in desiccated air. As will be shown later, even these precautions did not allow us to completely avoid surface contamination, which has an effect on the charge dynamics in the top layers. Therefore, the data presented in this paper differ somewhat from data presented in Ref. 23, although the same sample was used.

The real parts of the diagonal, $\sigma_{xx}(\omega)$, and Hall, $\sigma_{xy}(\omega)$, optical conductivities can be directly obtained from the magneto-optical absorption and Faraday rotation by using the general thin-film approximation, taking internal reflections in the substrate into account:

$$1 - T(\omega) \approx 2Z_0 f_s(\omega)\mathrm{Re}[\sigma_{xx}(\omega)], \quad (2)$$

$$\theta(\omega) \approx Z_0 f_s(\omega)\mathrm{Re}[\sigma_{xy}(\omega)], \quad (3)$$

where $Z_0 \approx 377\ \Omega$ is the impedance of vacuum and $f_s(\omega)$ is a spectrally smooth dimensionless function specific to the substrate.[23] These relations are obtained by linear expansion of the exact Fresnel formulas, which is accurate for our sample with only a few graphene layers. We reduced the spectral resolution to 1 meV in order to suppress the Fabry-Perot interference in the substrate. In this case,

$$f_s(\omega) = \frac{1}{n_s + 1} + \frac{2n_s}{n_s^2 - 1}\frac{q^2}{1 - q^2}, \quad (4)$$

where $q = [(n_s - 1)/(n_s + 1)]^2 \exp[-(2\omega/c)k_s d]$, and d, $n_s(\omega)$, and $k_s(\omega)$ are the thickness, the refractive index, and the extinction coefficient of the substrate. The latter quantities, which are independent of magnetic field, were determined from measurements of the absolute transmission and reflection spectra of the bare SiC at every temperature used.

The complex magneto-optical conductivity tensor

$$\hat{\sigma}(\omega) = \begin{bmatrix} \sigma_{xx}(\omega) & \sigma_{xy}(\omega) \\ -\sigma_{xy}(\omega) & \sigma_{xx}(\omega) \end{bmatrix} \quad (5)$$

is diagonal in the circular basis $\vec{x} \pm i\vec{y}$, with eigenvalues

$$\sigma_{\pm}(\omega) = \sigma_{xx}(\omega) \pm i\sigma_{xy}(\omega). \quad (6)$$

The absorption of right- and left-handed circular polarizations [which are shown in the insets of Figs. 1(c) and 1(d)] is described by the real parts of $\sigma_+(\omega)$ and $\sigma_-(\omega)$, respectively. This basis provides an intuitive way to present the magneto-optical conductivity showing individual LL transitions, which are active for strictly one circular polarization or the other.[24–26] In particular, for right circularly polarized light, transitions between electronlike LLs with $n \geqslant 0$, such as $\mathrm{LL}_{0\to1}$, $\mathrm{LL}_{1\to2}$, etc., are active, provided that the chemical potential is in between the corresponding LLs (the symbol $\mathrm{LL}_{i\to j}$ is used to designate the LL transition between levels i and j). Similarly, for left circularly polarized light, transitions between holelike LLs ($\mathrm{LL}_{-1\to0}$, $\mathrm{LL}_{-2\to-1}$, etc.) are excited.[27]

From Eq. (6) one can see that the imaginary part of $\sigma_{xy}(\omega)$ is needed to obtain the real part of the magneto-optical conductivity in the circular basis. Experimentally, $\mathrm{Im}[\sigma_{xy}(\omega)]$ is directly related to the ellipticity of the transmitted light. However, in the present experiment the error bars on the ellipticity are larger than the ones on the Faraday angle. Therefore, instead of directly applying Eq. (6) to the experimental data, we plot $\sigma_{\pm}(\omega)$ obtained from the results of the multicomponent fitting discussed in Sec. III A. For simplicity, in the rest of the paper, the symbols σ_{xx}, σ_{xy}, σ_+, and σ_- will be used to denote the real parts of the corresponding complex functions, unless stated otherwise.

III. RESULTS

A. Magneto-optical conductivity at 3 T and 5 K

Figure 1 shows representative conductivity spectra at $B = 3$ T and $T = 5$ K. The diagonal and Hall conductivities are plotted as solid lines in Figs. 1(a) and 1(b). They are expressed in dimensionless units of $\sigma_0 = e^2/4\hbar$, which is equal to the universal optical conductivity of monolayer graphene.[28] The rich structure of the spectra indicates the presence of multiple optical transitions. The absorption at low energy, shown by the arrow, corresponds to quasiclassical CR coming from the highly doped graphene layer closest to the SiC substrate.[23] At about 60 to 70 meV, a strong peak in $\sigma_{xx}(\omega)$ is observed that matches the energy of the $\mathrm{LL}_{0\to1}$ or $\mathrm{LL}_{-1\to0}$ transition at this field. The Hall conductivity displays a "zigzag" shape in this spectral range, suggesting that there are multiple components contributing to the optical response. In addition, a structure is present at about 27 meV, most clearly seen in $\sigma_{xy}(\omega)$, resulting from the $\mathrm{LL}_{1\to2}$ transition.

In order to disentangle different contributions to the magneto-optical spectra we used a multicomponent model

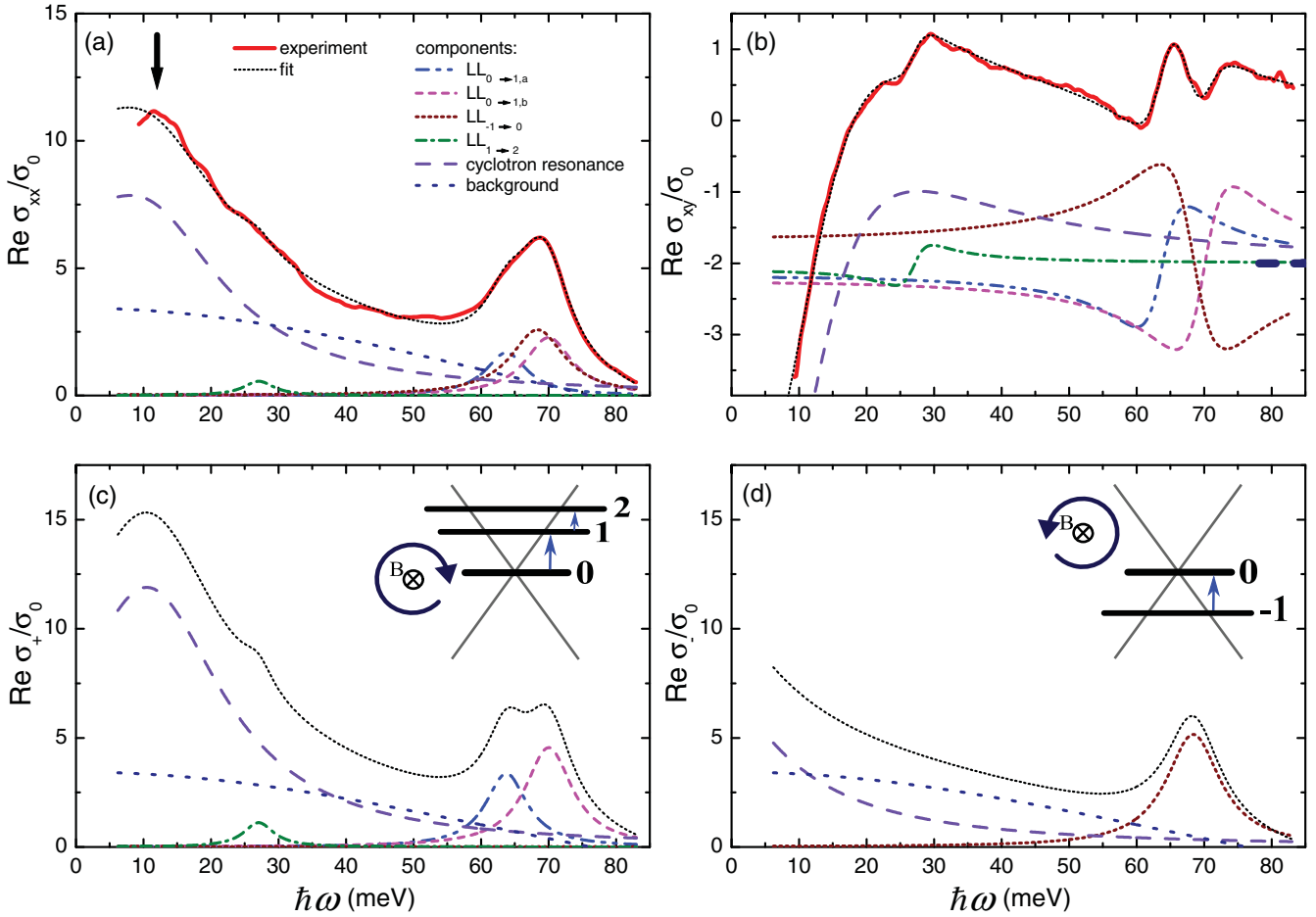

FIG. 1. (Color online) The diagonal (a) and Hall (b) optical conductivity at 3 T and 5 K, normalized to the universal conductivity σ_0, and results of the multicomponent modeling described in the text. The components in the graph are the individual contributions needed to create the total fit shown by the black dotted line on top of the data. The components in (b) have an offset indicated by the blue dashed line at the right side of the graph. (c),(d) The optical conductivities in the circular basis $\sigma_+(\omega)$ and $\sigma_-(\omega)$ corresponding to the absorption of right and left circular polarized light respectively. In the insets the low-index LL transitions allowed in the corresponding polarizations are shown.

where the total conductivity is given by the sum of separate cyclotron resonances. In the circular basis the total complex magneto-optical response is given by

$$\sigma_\pm(\omega) = \sum_j \frac{2W_j}{\pi} \frac{i}{\omega \mp \omega_{c,j} + i\gamma_j} \tag{7}$$

and the complex diagonal and Hall optical conductivities are accordingly expressed by

$$\sigma_{xx}(\omega) = \sum_j \frac{2W_j}{\pi} \frac{\gamma_j - i\omega}{\omega_{c,j}^2 - (\omega + i\gamma_j)^2}, \tag{8}$$

$$\sigma_{xy}(\omega) = \sum_j \frac{2W_j}{\pi} \frac{-\omega_{c,j}}{\omega_{c,j}^2 - (\omega + i\gamma_j)^2}, \tag{9}$$

where $\omega_{c,j}$ is the cyclotron frequency, W_j is the spectral weight, and γ_j is the broadening of the jth component. Physically speaking, each component can describe either a quasiclassical CR or a transition between individual LLs separated by energy $|\hbar\omega_{c,j}|$. Notably, $\sigma_{xx}(\omega)$ does not depend on the sign of the charge carriers, unlike $\sigma_{xy}(\omega)$, where the sign can be derived directly from the spectral shape.[23] In $\sigma_{xx}(\omega)$ each component results in a peak centered at $|\omega_{c,j}|$. In $\sigma_{xy}(\omega)$, however, it shows an antisymmetric structure, where $|\omega_{c,j}|$ corresponds to the inflection point in the curve. The slope at this point coincides with the sign of the cyclotron frequency and reveals the polarity of the charge carriers involved in the transition.[23] In particular, a positive (negative) slope signals electronlike (holelike) carriers.

The spectra $\sigma_{xx}(\omega)$ and $\sigma_{xy}(\omega)$ were simultaneously fitted using Eqs. (8) and (9), while allowing the parameters $\omega_{c,j}$, W_j, and γ_j to change freely. The fitting curves are shown in Figs. 1(a) and 1(b), as black dotted lines. We found that a minimal model describing satisfactorily the spectral structures contains six components, which are shown separately in the same panels.

Interestingly, it was necessary to introduce at least three components with transition energies between 60 and 70 meV to describe the structure in this range. Two of the resonances are electronlike, which we designate as $\mathrm{LL}_{0\to1,a}$ and $\mathrm{LL}_{0\to1,b}$, and one is holelike, referred to as $\mathrm{LL}_{-1\to0}$. Note that all these transitions are actually at different energies, which is clearly seen already from the presence of three inflection points in the optical Hall conductivity. A fourth

component is at about 27 meV and corresponds to the electronlike $LL_{1\to2}$ transition. The fifth component with a small value of $\hbar\omega_c = 9$ meV originates from a quasiclassical electronlike CR. Finally, there is a component with zero cyclotron frequency and large scattering, which forms a broad absorption background present in $\sigma_{xx}(\omega)$, but absent in $\sigma_{xy}(\omega)$. A possible origin of this background will be discussed in Sec. IV.

The different contributions from electrons and holes to the magneto-optical conductivity are easily seen in the basis of circularly polarized light as shown in Figs. 1(c) and 1(d). The electronlike transitions $LL_{0\to1,a}$, $LL_{0\to1,b}$, and $LL_{1\to2}$ as well as the CR show peaks in $\sigma_+(\omega)$, while the holelike $LL_{-1\to0}$ transition manifests itself in $\sigma_-(\omega)$. Because of the small value of ω_c and a relatively large scattering, the CR component also has a tail in $\sigma_-(\omega)$. The absorption background contributes equally to $\sigma_+(\omega)$ and $\sigma_-(\omega)$.

B. Dependence on magnetic field

The magnetic field dependence of $\sigma_{xx}(\omega)$ and $\sigma_{xy}(\omega)$, measured at 5 K, is shown in Figs. 2(a) and 2(b). The multicomponent character of the spectra is present at different fields, although the resonances show a strong field dependence. The model described in Sec. III A was used to fit $\sigma_{xx}(\omega)$ and $\sigma_{xy}(\omega)$ simultaneously for every field. The fits, shown as black dotted lines, are used to calculate the magneto-optical conductivities in the bases of right- and left-handed circularly polarized light according to Eq. (7), and these are plotted in Figs. 2(c) and 2(d).

The field dependence of all fitting parameters is shown in Fig. 3. The energy of the CR is linear in field, as seen in Fig. 3(a). This quasiclassical behavior is expected for highly doped graphene, where large-index LLs are close to the Fermi energy.[28,29] In this case the quasiclassical cyclotron frequency is inversely proportional to the Fermi energy ϵ_F:

$$\omega_c = \frac{|e|Bv_F^2}{\epsilon_F}. \tag{10}$$

Using this relation and taking as an estimate $v_F = 1.0 \times 10^6$ m/s, we obtain $\epsilon_F = 0.24$ eV, which corresponds to a carrier concentration $n = \epsilon_F^2/\pi v_F^2\hbar^2 = 4.2 \times 10^{12}$ cm^{-2}.

The spectral weight W of the cyclotron peak, shown in Fig. 3(d), is field independent within the experimental accuracy. In the absence of interactions, the Drude weight in a single graphene layer is related to ϵ_F by the formula

$$\frac{\hbar W}{\sigma_0} = 2|\epsilon_F|. \tag{11}$$

This gives $\epsilon_F = 0.16$ eV and accordingly $n = 1.9 \times 10^{12}$ cm^{-2}, which are significantly smaller than the values based on the cyclotron frequency. It is possible that interactions renormalize the Drude weight and spread the missing weight over a large spectral range. In our fits this missing weight might be "absorbed" by the broad background component mentioned above. On the other hand, we obtain a reduced Drude weight based on the assumption that for the bottom layer $v_F = 1.0 \times 10^6$ m/s. Accepting a smaller Fermi velocity (by about 20%) would make the cyclotron resonance and the Drude weight match according to Eqs. (10) and (11).

The scattering rate $\hbar\gamma$ [Fig. 3(g)] of the cyclotron peak is field independent and equal to about 14 meV. Using the semiclassical relation

$$\mu = \frac{|\omega_c|}{\gamma|B|}, \tag{12}$$

we find a mobility of about 2000 cm^2/V s, based on the experimental values of the scattering rate and the cyclotron

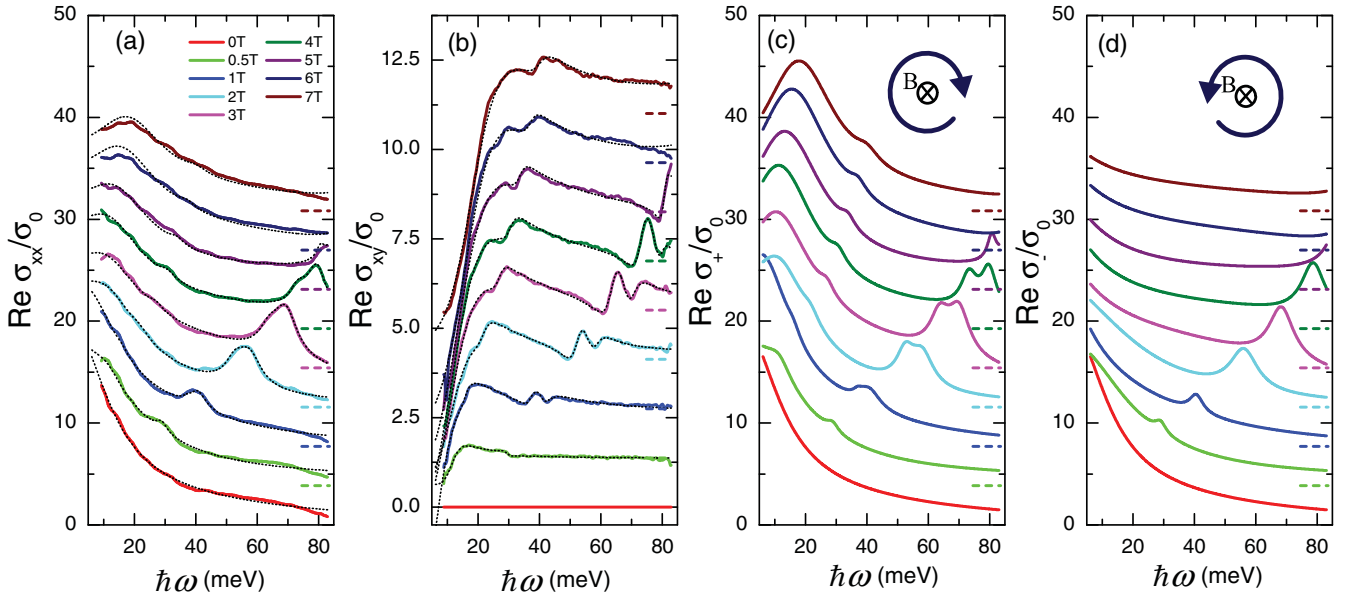

FIG. 2. (Color online) Magneto-optical conductivity of multilayer graphene at 5 K, normalized to the universal conductivity σ_0, for several magnetic fields up to 7 T. The curves in all panels are offset as indicated by the dashed lines. Larger offsets correspond to higher magnetic fields. (a) and (b) show the measured spectra of $\sigma_{xx}(\omega)$ and $\sigma_{xy}(\omega)$ (solid lines) and multicomponent fits (black dotted lines). In (c) and (d) the model-derived $\sigma_+(\omega)$ and $\sigma_-(\omega)$ are shown.

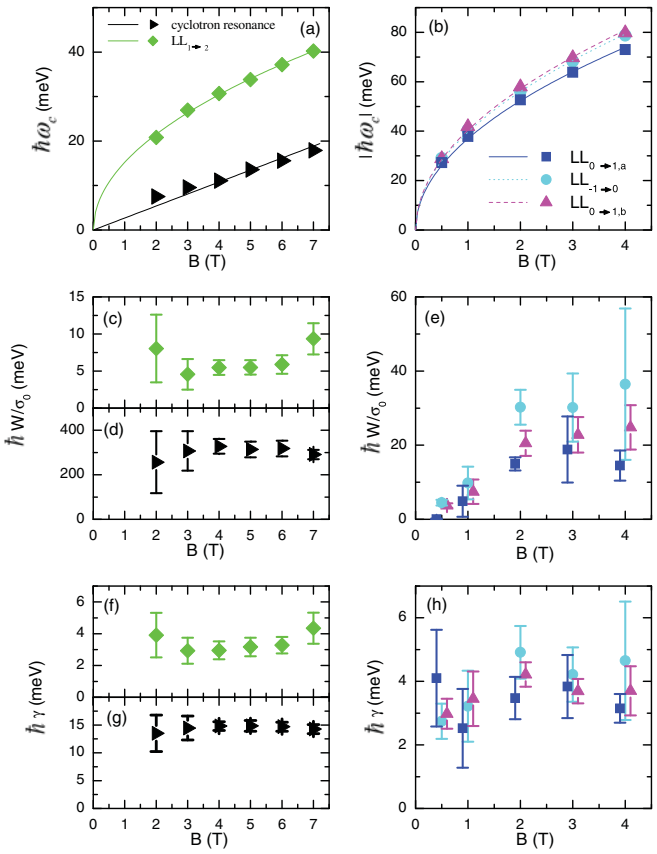

FIG. 3. (Color online) Parameters of various components as a function of magnetic field obtained from the multicomponent fits to $\sigma_{xx}(\omega)$ and $\sigma_{xy}(\omega)$ of Fig. 2. (a) The transition energies of the CR (triangles) and the $LL_{1\to2}$ transition (diamonds). The solid lines are fits using Eqs. (10) and (1), respectively. (b) The transition energies of $LL_{0\to1,a}$ (squares), $LL_{0\to1,b}$ (triangles), and $LL_{-1\to0}$ (circles) transitions. The solid lines are fits using Eq. (1). (c) Spectral weight of the $LL_{1\to2}$ transition. (d) Spectral weight of the CR peak. (e) Spectral weights of the $LL_{0\to1,a}$, $LL_{0\to1,b}$, and $LL_{-1\to0}$ transitions. (f) The broadening of the $LL_{1\to2}$ transition. (g) The broadening of the CR transition. (h) The broadening of $LL_{0\to1,a}$, $LL_{0\to1,b}$, and the $-1\to0$ transitions. Error bars in all figures are the standard deviation of several fitting results. The error bars in (a) and (b) are within the symbol size.

frequency. Magnetotransport measurements show that the carrier density and mobility in multilayer graphene are correlated.[30] The values of n and μ that we obtain here for the CR fall on the generic dependence found in Ref. 30. CR was also observed in monolayer epitaxial graphene on the silicon side of silicon carbide,[23,31] where similar mobility of carriers was found.[23]

Next we discuss the field dependence of the LL transitions. From $\sigma_+(\omega)$ and $\sigma_-(\omega)$ it is particularly evident that the two electronlike and one holelike resonances described above have a similar magnetic field dependence. The energies of all low-index LL transitions, namely, $LL_{1\to2}$ [Fig. 3(a)], $LL_{0\to1,a}$, $LL_{0\to1,b}$, and $LL_{-1\to0}$ [Fig. 3(b)] clearly follow the square-root dependence on magnetic field typical of massless Dirac fermions [Eq. (1)], in accordance with previous observations in similar epitaxial graphene samples[9] and exfoliated monolayer

TABLE I. Fermi velocities found for different LL transitions.

Transition	v_F (m/s)
$LL_{0\to1,a}$	1.02×10^6
$LL_{0\to1,b}$	1.11×10^6
$LL_{-1\to0}$	1.09×10^6
$LL_{1\to2}$	1.01×10^6

flakes.[32,33] Fitting the field dependence of the LL transition energies using Eq. (1) provides the Fermi velocities listed in Table I; they show a spread of about 10%. The difference between the Fermi velocities found from the electronlike $LL_{0\to1,b}$ and holelike $LL_{-1\to0}$ transitions is only about 2%. However, the presence of three distinct inflection points in $\sigma_{xy}(\omega)$ corresponding to the energies of the three LL transitions is a clear sign that the transition energies and therefore the Fermi velocities are different.

The spectral weights of the $LL_{1\to2}$, $LL_{0\to1,a}$, $LL_{0\to1,b}$, and $LL_{-1\to0}$ transitions increase with magnetic field [Figs. 3(d) and 3(e)]. This is in qualitative agreement with an increase of the number of states within each LL with magnetic field.[9,34] However, a closer look at the absolute values of the spectral weights reveals a strong reduction with respect to the theoretical expectation for ideal graphene monolayers, as discussed in Sec. IV.

The scattering rate of the LL transitions is about 3 to 4 meV and magnetic field independent [Figs. 3(f) and 3(h)]. Although in the case of the cyclotron peak we extracted the mobility using the scattering rate and the cyclotron frequency, in the quantum limit, where the transition energy is proportional to $\sqrt{B}$, the quasiclassical Eq. (12) will formally result in diverging mobility values at low fields.

C. Temperature dependence

The temperature dependence of $\sigma_{xx}(\omega)$ and $\sigma_{xy}(\omega)$ at a fixed field of 3 T is shown in Figs. 4(a) and 4(b), respectively. In both sets of curves, the CR structure changes weakly with temperature. The situation is different for the LL transitions. In $\sigma_{xx}(\omega)$ the LLs are preserved at all temperatures, although at elevated temperatures the peaks are about 3 meV broader than at low temperatures as obtained from the fits shown in the same graphs. Their spectral weight is almost temperature independent. However, in $\sigma_{xy}(\omega)$, the spectral features corresponding to the LL transitions are strongly diminished at high temperatures and almost disappear at room temperature.

The extinction of the spectral structures corresponding to the LL transitions in $\sigma_{xy}(\omega)$ on warming is due to the simultaneous presence of electron- and holelike LL transitions as seen in the graphs of $\sigma_+(\omega)$ and $\sigma_-(\omega)$, plotted in Figs. 4(c) and 4(d). At high temperatures, the electron- and holelike components that have slightly different Fermi velocities overlap more, due to the increased broadening. In $\sigma_{xy}(\omega)$ the contributions are subtractive and more overlap results in weaker spectral structures. On the other hand, in $\sigma_{xx}(\omega)$, which is insensitive to the sign of the charge carriers, the contributions are additive and the transition peak appears less affected.

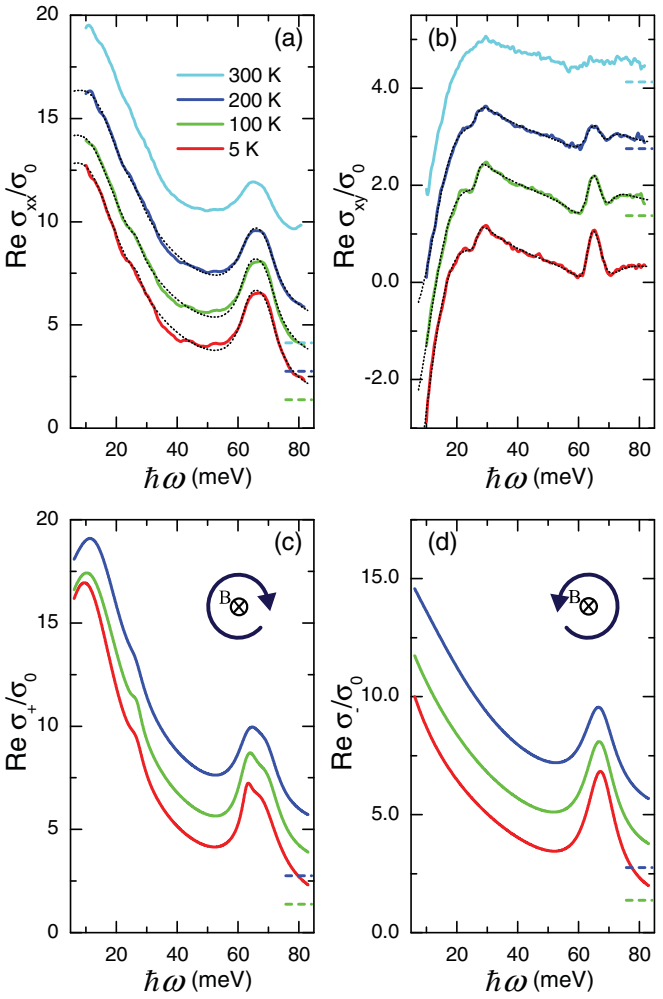

FIG. 4. (Color online) Magneto-optical conductivity of multilayer graphene at 3 T, normalized to the universal conductivity σ_0, for several temperatures between 5 and 300 K. The curves in all panels are offset as indicated by the dashed lines. Larger offsets correspond to higher temperatures. (a) and (b) show the measured spectra of $\sigma_{xx}(\omega)$ and $\sigma_{xy}(\omega)$ (solid lines) and multicomponent fits (black dotted lines, only at 5, 100, and 200 K). In (c) and (d) the model-derived $\sigma_+(\omega)$ and $\sigma_-(\omega)$ are shown.

D. Effects of environmental doping

A careful inspection of the two series of measurements (Figs. 2 and 4) shows that the spectra from the different series taken at the same experimental conditions (5 K and 3 T) are not precisely the same, especially close to the $LL_{0\to1,a}$, $LL_{0\to1,b}$, and $LL_{-1\to0}$ transition energies. As was mentioned above, between these measurements the sample was held in dry air; therefore it is reasonable to assume that the difference is due to the effect of environmental molecular contamination.[35] In the case of multilayer graphene, the electronic properties of the outmost layer are most strongly modified, although one cannot exclude a certain effect on inner layers as well.

Figure 5(a) shows the contributions of the $LL_{0\to1,a}$ and $LL_{0\to1,b}$ transitions to $\sigma_+(\omega)$, for both measurements at 5 K and 3 T. The low-energy $LL_{0\to1,a}$ transition with $v_F = 1.02 \times 10^6$ m/s is unaltered. The high-energy $LL_{0\to1,b}$ transition with $v_F = 1.11 \times 10^6$ m/s, however, shows a clear change:

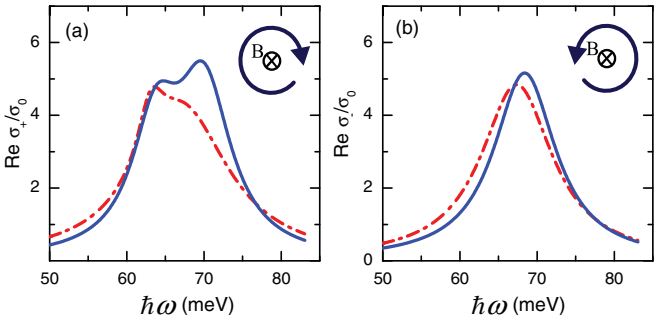

FIG. 5. (Color online) The effect of environmental doping on the LL transitions at $B = 3$ T and $T = 5$ K. (a) The contributions of the $LL_{0\to1,a}$ and $LL_{0\to1,b}$ transitions to $\sigma_+(\omega)$. (b) The contribution of the $LL_{-1\to0}$ transition to $\sigma_-(\omega)$. In both panels, the red dash-dotted lines correspond to the measurement series as a function of temperature at constant magnetic field (Fig. 4), while the blue solid lines correspond to the measurement series as a function of magnetic field at constant temperature (Fig. 2). The curves are derived from the multicomponent fits of experimental data.

the structure is much sharper in the second measurement. In Fig. 5(b) the contribution of the $LL_{-1\to0}$ transition to $\sigma_-(\omega)$ is plotted for both measurements. Similarly to $LL_{0\to1,b}$, it shows a sharpening in the second measurement. The fact that both $LL_{0\to1,b}$ and $LL_{-1\to0}$ transition peaks are changed with environmental doping suggests that these transitions originate from the bands in the outmost graphene layer, which is most affected by surface contamination. The $LL_{0\to1,a}$ transition with the lowest v_F is unchanged by the environmental doping, therefore it probably comes from deeper graphene layers.

Figure 3(e) shows that the spectral weights of the $LL_{0\to1,b}$ and $LL_{-1\to0}$ transitions are approximately equal, which indicates a balance between electrons and holes in the top layer. The Fermi velocity of the electrons (1.11×10^6 m/s) in that layer is slightly larger than the one of the holes (1.09×10^6 m/s). Similar results were found for monolayer exfoliated[33] and few-layer chemical-vapor-deposited[36] graphene. The electron-hole asymmetry in our work (about 2%) is much smaller than that found in Ref. 36, which might be due to different rotation angles between the layers in the samples used. Indeed, the asymmetry between electrons and holes was experimentally shown to depend on the relative rotation between successive graphene layers,[36] where a large (small) rotation between the layers gives a small (large) asymmetry.

IV. DISCUSSION

Multilayer graphene on the C side of SiC is often regarded as a stack of twisted monolayers, electronically decoupled from each other due to random rotational stacking, where the doping level varies across the layers due to the effects of the substrate and the surface contamination. Our observation of the CR and the LL transitions ($LL_{1\to2}$, $LL_{0\to1}$, $LL_{-1\to0}$) in the same spectra is a clear indication of this doping variation. Indeed, since only transitions between occupied and empty states can occur, their simultaneous activation implies different positions of the chemical potential with respect to the Dirac-point energy. However, the activation of

different LL transitions may also be caused by a spatial doping inhomogeneity.

The nearly perfect square-root dependence of the LL transition energies on magnetic field found in previous work[9,26] and confirmed by the present measurements [Figs. 2(a) and 2(b)] is a signature of massless Dirac dispersion inherent to monolayer graphene. The same field dependence of LLs is obtained by STM.[10,11] Accordingly, ARPES measurements[12] show multiple Dirac cones from individual layers. However, a number of our observations are difficult to fit into a simple picture of completely isolated monolayers. One of them is a significant (about 10%) spread of the Fermi velocity in the same sample. The largest values $v_F = (1.09–1.11) \times 10^6$ m/s we attribute to the outermost graphene layer, based on the effect of the surface contamination, while the smallest values, $v_F = (1.01–1.02) \times 10^6$ m/s, correspond to the inner layers, where the transitions $LL_{0\to1,a}$ and $LL_{1\to2}$ are active due to a weak electron doping. It was theoretically predicted[16,18,19] that in rotationally stacked graphene layers the effect of the interlayer interaction is to reduce the Fermi velocity with respect to its "bare" value in monolayer graphene. The variation of v_F that we find can thus be attributed to the effect of layer twisting and a randomness of the rotation angles between various layers.

It is important to compare not only the energies but also the optical spectral weights W of the LL transitions with theoretical expectations.[24,34] Experimentally, we obtain the weights from the multicomponent spectral fitting, described in Sec. III A. Let us consider the spectral weights of the $LL_{0\to1}$ and $LL_{-1\to0}$ transitions. Assuming that the chemical potential is between the first electron and hole LLs (E_{-1} and E_1), the total weight of these transitions in monolayer graphene is given, according to the Kubo formalism for noninteracting Dirac fermions, by the transition energy itself:[34]

$$\hbar W/\sigma_0 = 2(E_1 - E_0) = 2\sqrt{2e\hbar v_F^2|B|}. \qquad (13)$$

This dependence on magnetic field for $v_F = 1.0 \times 10^6$ m/s is plotted in Fig. 6 as a solid line. The symbols show the sum of the experimental spectral weights of the $LL_{0\to1,a}$, $LL_{0\to1,b}$, and $LL_{-1\to0}$ transitions. The experimental points are clearly below the theoretical curve. From here it follows that even if only one graphene layer has the chemical potential between E_{-1} and E_1 then the total spectral weight observed is about two times smaller than the theoretical expectation. In reality it is likely that the number of layers in the present sample that satisfy the condition for the chemical potential is larger, which would make the deviation even stronger.

A possibly related experimental observation is the presence of the optical absorption background found from the fitting results of the phenomenological cyclotron multicomponent model. This component, with vanishing ω_c, has a substantial spectral weight spread over a broad frequency range. The existence of the background shows that a significant amount of the charge carriers in the graphene layers do not fall into well-defined either CR or LL transitions and signals a departure from the isolated monolayer description. In terms of the optical sum rule, the missing spectral weight of the LL transitions is transferred to the background. An intriguing question is whether this transfer is caused by interlayer coupling or by many-body effects within individual layers, such as electron-electron and electron-phonon interactions.

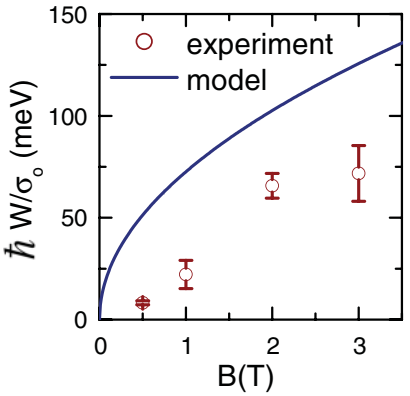

FIG. 6. (Color online) Total spectral weight of the $LL_{0\to1,a}$, $LL_{0\to1,b}$, and $LL_{-1\to0}$ transitions (circles) as compared to the theoretical prediction for the spectral weight of the sum of the $LL_{0\to1}$ and $LL_{-1\to0}$ transitions in ideal monolayer graphene (solid line) with the chemical potential between E_{-1} and E_1.

One should notice that the mobility and density of carriers in epitaxial graphene show a large variation from sample to sample, even when they are prepared under similar conditions.[30] This shows that the interlayer twist angle, which is at the moment difficult to control experimentally, is a crucial parameter affecting the electronic and therefore optical properties of epitaxial graphene.

V. CONCLUSIONS

Using magneto-optical infrared Hall spectroscopy, the charge dynamics in multilayer epitaxial graphene grown on the C side of SiC was studied in magnetic fields up to 7 T. The diagonal and the Hall conductivities were extracted from the absorption and the Faraday rotation spectra, respectively. The latter is sensitive to the sign of charge carriers, which allowed us to distinguish between electron- and holelike transitions. The mobility and charge density of electrons were found, which makes this technique a useful contactless characterization tool.

A general multicomponent model, Eq. (7), provided excellent fits at each field to $\sigma_{xx}(\omega)$ and $\sigma_{xy}(\omega)$ simultaneously. This analysis revealed the coexistence of optical transitions between individual LLs with a square-root dependence of the transition energies on magnetic field, as expected for isolated monolayer graphene, and a quasiclassical CR showing a linear magnetic field dependence. This is a clear indication of the doping variation across the layers.

We find the simultaneous presence of at least two distinct peaks due to transitions between Landau levels 0 and 1 (electrons). The separation between these peaks corresponds to a difference between the Fermi velocities of about 10%. One more peak due to a transition between LLs −1 (holes) and 0 is observed. The effect of the surface contamination on the spectra shows that both electrons and holes are present in the top layer and that the electrons have slightly higher Fermi velocity than the holes (by 2%). The variation of the

Fermi velocity is probably related to random twisting angles between graphene layers.

The spectral weight of the LL transitions is shown to be significantly reduced with respect to the theoretical expectation for a stack of fully decoupled graphene monolayers, assuming the picture of noninteracting electrons within each layer. This missing spectral weight correlates with the presence of an unexpected broadband optical absorption, which is also inconsistent with this simplified theoretical model.

Although the transition energies of the LL transitions clearly follow the magnetic field dependence expected for isolated graphene, in order to come to a complete picture of the complex electronic structure of multilayer graphene we need to understand the variation of the Fermi velocity, the small optical spectral weight of the LL transition, and the broad absorption background in relation to the twist angle of the layers. Therefore, a systematic study of samples where this angle is experimentally controlled is required.

ACKNOWLEDGMENTS

This work was supported by the Swiss National Science Foundation (SNSF) by Grants No. 200021-120347 and No. IZ73Z0-128026 (SCOPES program), through the National Centre of Competence in Research 'Materials with Novel Electronic Properties-MaNEP'. We thank S. G. Sharapov for useful discussions.

[1] C. Berger, Z. Song, T. Li, X. Li, A. Y. Ogbazghi, R. Feng, Z. Dai, A. N. Marchenkov, E. H. Conrad, P. N. First, and W. A. de Heer, J. Phys. Chem. B **108**, 19912 (2004).

[2] C. Berger, Z. Song, X. Li, X. Wu, N. Brown, C. Naud, D. Mayou, T. Li, J. Hass, A. N. Marchenkov, E. H. Conrad, P. N. First, and W. A. de Heer, Science **312**, 1191 (2006).

[3] K. V. Emtsev, A. Bostwick, K. Horn, J. Jobst, G. L. Kellogg, L. Ley, J. L. McChesney, T. Ohta, S. A. Reshanov, J. Röhrl, E. Rotenberg, A. K. Schmid, D. Waldmann, H. B. Weber, and Th. Seyller, Nature Mater. **8**, 203 (2009).

[4] A. Tzalenchuk, S. Lara-Avila, A. Kalaboukhov, S. Paolillo, M. Syväjärvi, R. Yakimova, O. Kazakova, J. B. M. Janssen, V. Fal'lko, and S. Kubatkin, Nature Nano. **5**, 186 (2010).

[5] C. Riedl, C. Coletti, T. Iwasaki, A. A. Zakharov, and U. Starke, Phys. Rev. Lett. **103**, 246804 (2009).

[6] F. Speck, M. Ostler, J. Röhrl, J. Jobst, D. Waldmann, M. Hundhausen, L. Ley, H. B. Weber, and Th. Seyller, Mater. Sci. Forum **645**, 629 (2010).

[7] P. N. First, W. A. de Heer, Th. Seyller, C. Berger, J. A. Stroscio, and J.-S. Moon, MRS Bull. **35**, 296 (2010).

[8] J. Hass, F. Varchon, J. E. Millán-Otoya, M. Sprinkle, N. Sharma, W. A. de Heer, C. Berger, P. N. First, L. Magaud, and E. H. Conrad, Phys. Rev. Lett. **100**, 125504 (2008).

[9] M. L. Sadowski, G. Martinez, M. Potemski, C. Berger, and W. A. de Heer, Phys. Rev. Lett. **97**, 266405 (2006).

[10] D. L. Miller, K. D. Kubista, G. M. Rutter, M. Ruan, W. A. de Heer, P. N. First, and J. A. Stroscio, Science **324**, 924 (2009).

[11] Y. J. Song, A. F. Otte, Y. Kuk, Y. Hu, D. B. Torrance, P. N. First, W. A. de Heer, H. Min, S. Adam, M. D. Stiles, A. H. MacDonald, and J. A. Stroscio, Nature (London) **467**, 185 (2010).

[12] M. Sprinkle, D. Siegel, Y. Hu, J. Hicks, A. Tejeda, A. TalebIbrahimi, P. Le Fèvre, F. Bertran, S. Vizzini, H. Enriquez, S. Chiang, P. Soukiassian, C. Berger, W. A. de Heer, A. Lanzara, and E. H. Conrad, Phys. Rev. Lett. **103**, 226803 (2009).

[13] X. Wu, Y. Hu, M. Ruan, N. K. Madiomanana, J. Hankinson, M. Sprinkle, C. Berger, and W. A. de Heer, Appl. Phys. Lett. **95**, 223108 (2009).

[14] F. Guinea, A. H. Castro Neto, and N. M. R. Peres, Phys. Rev. B **73**, 245426 (2006).

[15] E. McCann and V. I. Fal'ko, Phys. Rev. Lett. **96**, 086805 (2006).

[16] J. M. B. Lopes dos Santos, N. M. R. Peres, and A. H. Castro Neto, Phys. Rev. Lett. **99**, 256802 (2007).

[17] S. Shallcross, S. Sharma, and O. A. Pankratov, Phys. Rev. Lett. **101**, 056803 (2008).

[18] G. T. de Laissardière, D. Mayou, and L. Magaud, Nano Lett. **10**, 804 (2010).

[19] S. Shallcross, S. Sharma, E. Kandelaki, and O. A. Pankratov, Phys. Rev. B **81**, 165105 (2010).

[20] E. J. Mele, Phys. Rev. B **81**, 161405 (2010).

[21] R. Bistritzer and A. H. MacDonald, Phys. Rev. B **81**, 245412 (2010).

[22] R. Bistritzer and A. H. MacDonald, e-print arXiv:1101.2606.

[23] I. Crassee, J. Levallois, A. L. Walter, M. Ostler, A. Bostwick, E. Rotenberg, Th. Seyller, D. van der Marel, and A. B. Kuzmenko, Nature Phys. **7**, 48 (2011).

[24] D. S. L. Abergel and V. I. Fal'ko, Phys. Rev. B **75**, 155430 (2007).

[25] V. P. Gusynin, S. G. Sharapov, and J. P. Carbotte, J. Phys.: Condens. Matter **19**, 026222 (2007).

[26] M. Orlita and M. Potemski, Semicond. Sci. Technol. **25**, 06001 (2010).

[27] Note that also transitions between electron- and holelike LLs are optically allowed. However, for the magnetic fields used, these transitions are beyond the experimental spectral range, except at 0.5 T, where rather weak contributions from $LL_{-1\to 2}$ and $LL_{-2\to 1}$ could be discerned.

[28] T. Ando, Y. Zheng, and H. Suzuura, J. Phys. Soc. Jpn. **71**, 1318 (2002).

[29] V. P. Gusynin, S. G. Sharapov, and J. P. Carbotte, New J. Phys. **11**, 095013 (2009).

[30] M. Y. Lin, C. Dimitrakopoulos, D. B. Farmer, S.-J. Han, Y. Wu, W. Zhu, D. K. Gaskill, J. L. Tedesco, R. L. Myers-Ward, C. R. Eddy, A. Grill, and P. Avouris, Appl. Phys. Lett. **97**, 112107 (2010).

[31] A. M. Witowski, M. Orlita, R. Stpniewski, A. Wysmołek, J. M. Baranowski, W. Strupiński, C. Faugeras, G. Martinez, and M. Potemski, Phys. Rev. B **82**, 165305 (2010).

[32] Z. Jiang, E. A. Henriksen, L. C. Tung, Y.-J. Wang, M. E. Schwartz, M. Y. Han, P. Kim, and H. L. Stormer, Phys. Rev. Lett. **98**, 197403 (2007).

[33] R. S. Deacon, K.-C. Chuang, R. J. Nicholas, K. S. Novoselov, and A. K. Geim, Phys. Rev. B **76**, 081406(R) (2007).

[34] V. P. Gusynin, S. G. Sharapov, and J. P. Carbotte, Phys. Rev. Lett. **98**, 157402 (2007).

[35] F. Schedin, A. K. Geim, S. V. Morozov, E. W. Hill, P. Blake, M. I. Katsnelson, and K. S. Novoselov, Nature Mater. **6**, 652 (2007).

[36] A. Luican, G. Li, A. Reina, J. Kong, R. R. Nair, K. S. Novoselov, A. K. Geim, and E. Y. Andrei, Phys. Rev. Lett. **106**, 126802 (2011).